# Hadron structure with light dynamical quarks

**Robert G. Edwards**

*Thomas Jefferson National Accelerator Facility, Newport News, VA 23606, USA*

**George T. Fleming**

*Sloane Physics Laboratory, Yale University, New Haven, CT 06520, USA*

**Philipp Hägler**

*Department of Physics and Astronomy, Vrije Universiteit, 1081 HV Amsterdam, NL*

**John W. Negele**

*Center for Theoretical Physics, Massachusetts Institute of Technology, Cambridge, MA 02139, USA*

**Kostas Orginos**

*Center for Theoretical Physics, Massachusetts Institute of Technology, Cambridge, MA 02139, USA*

**Andrew Pochinsky**

*Center for Theoretical Physics, Massachusetts Institute of Technology, Cambridge, MA 02139, USA*

**Dru B. Renner**

*Department of Physics, University of Arizona, 1118 E 4th Street, Tucson, AZ 85721, USA*

**David G. Richards**

*Thomas Jefferson National Accelerator Facility, Newport News, VA 23606, USA*

**Wolfram Schroers**[*]

*John von Neumann-Institut für Computing NIC/DESY, 15738 Zeuthen, Germany*

Generalized parton distributions encompass a wealth of information concerning the three-dimensional quark and gluon structure of the nucleon, and thus provide an ideal focus for the study of hadron structure using lattice QCD. The special limits corresponding to form factors and parton distributions are well explored experimentally, providing clear tests of lattice calculations, and the lack of experimental data for more general cases provides opportunities for genuine predictions and for guiding experiment. We present results from hybrid calculations with improved staggered (Asqtad) sea quarks and domain wall valence quarks at pion masses down to 350 MeV.

*XXIIIrd International Symposium on Lattice Field Theory*
*25-30 July 2005*
*Trinity College, Dublin, Ireland*

---

[*]Combined proceedings of G.T. Fleming, D.B. Renner, and W. Schroers
[†]Speaker.

## 1. Introduction

The discovery of generalized parton distributions (GPDs) (see [1] for the pioneering articles and [2] for recent comprehensive reviews) for the characterization of both exclusive and inclusive reactions has stirred new interest in both experimentalists and theoreticians. For the first time it was possible not only to describe seemingly unrelated processes in terms of a single set of functions characterizing a hadron, but also to incorporate information that was not available before. The ability to compute the total quark contribution to the nucleon spin [3] plays on important role in resolving the spin crisis.

These developments provide an ideal opportunity for contemporary lattice QCD. While these calculations are still limited to quark masses heavier than in nature they can provide invaluable qualitative insight into the mechanisms of QCD. The pioneering lattice works on this field were published simultaneously by the QCDSF [4] and LHPC [5] collaborations. Already these early papers are playing an important role in phenomenology [6].

Later lattice investigations have unraveled important information on the transverse structure of the nucleon [7], polarized processes [8] and the tensor structure of GPDs [9]. The role of lattice QCD is of particular importance in this young field since the GPDs are inherently more complicated than form factors or parton distributions alone. Several of these functions can only be determined from lattice calculations and are not directly accessible to experiments.

This paper focuses on the application of hybrid lattice calculations [10] to the lowest moments of the GPDs. It is organized as follows. After an introduction to the parameterization of GPDs in section 2, we outline the current status of our hybrid calculations in section 3. We present the preliminary results from our calculations in section 5 which covers the electromagnetic form factors and the nucleon energy-momentum tensor. In the forward limit the GPDs reduce to the moments of forward parton-distributions for which a plethora of detailed experimental data is available. For this reason, we discuss this case in more detail in section 4. Finally, we present an outlook to the analysis of form factors at large momentum transfer in section 6. We close with our plans for future calculations to complete our program in section 7.

## 2. Generalized parton distributions

In the following, we focus on the case of a nucleon. Naturally, GPDs can be defined for all other hadrons as well. For the case of the pion, see [11] in these proceedings. Generalized parton distributions are defined by the nucleon matrix element of an operator that creates and annihilates quarks separated by a given distance on the light cone:

$$\bar{p}^+ \int \frac{dz^-}{2\pi} e^{\mathrm{i}\bar{p}^+ z^-} \langle p'|\bar{\psi}(-z^-/2)\Gamma\psi(z^-/2)|p\rangle \tag{2.1}$$

with $p$ being the momentum of the incoming, and $p'$ being the momentum of the outgoing nucleon. The average nucleon momentum is $\bar{p} = 1/2(p' + p)$. These matrix elements can be parameterized by functions depending on three kinematic variables, the average longitudinal momentum fraction, $x$, the skewness, $\xi$, and the total spacelike virtual momentum transfer, $Q^2 \equiv t = (p' - p)^2$. Additionally, the GPDs implicitly depend also on a renormalization scale, $\mu^2$. This scale fixes the scale

| $\Gamma$ | Function | Meaning |
|---|---|---|
| $\gamma^\mu$ | $H(x,\xi,t), E(x,\xi,t)$ | Spin-independent |
| $\gamma_5\gamma^\mu$ | $\tilde{H}(x,\xi,t), \tilde{E}(x,\xi,t)$ | Spin-dependent |
| $\sigma^{\rho\mu}\gamma^\nu$ | $H_T(x,\xi,t), E_T(x,\xi,t),$ | Transverse |
| | $\tilde{H}_T(x,\xi,t), \tilde{E}_T(x,\xi,t)$ | |

**Table 1:** List of fermion GPDs for the nucleon.

of the struck quark when using GPDs in a factorization scheme. Depending on the Dirac structure, $\Gamma$, in Eq. (2.1) there are in total eight GPD functions. These functions are summarized in table 1.

Since we cannot compute non-local matrix elements in the Euclidean regime where lattice calculations are performed, we have to compute moments with respect to the longitudinal momentum fraction, $x$. These moments are obtained by performing a light-cone operator product expansion. The resulting moments will then be polynomials in $(2\xi)^2$. The coefficient functions are the so-called generalized form factors (GFFs). In this paper, we restrict ourselves to moments as high as the energy-momentum tensor of QCD. The parameterization takes on the following form:

$$\int dx H(x,\xi,t) = A_{10}(t) = F_1(t), \quad \int dx E(x,\xi,t) = B_{10}(t) = F_2(t), \tag{2.2}$$

$$\int dx x H(x,\xi,t) = A_{20}(t) - (2\xi)^2 C_2(t), \quad \int dx x E(x,\xi,t) = B_{20}(t) + (2\xi)^2 C_2(t). \tag{2.3}$$

The zeroth moment corresponds to the regular electromagnetic form factors, while the first moment corresponds to the energy-momentum tensor. Furthermore, we restrict ourselves to the flavor combination up minus down since in this case the flavor-singlet parts involving disconnected diagrams cancel due to isospin symmetry.

## 3. Hybrid lattice calculations

The basic shortcoming of most currently employed lattice fermion actions is their enormous cost which makes calculations with sufficiently light sea quarks prohibitively expensive. The principal idea behind hybrid calculation consists of using different types of fermion actions for the sea quarks — the virtual quark and anti-quark pairs created from loops from the gluon propagator — and the valence quarks which connect to the source and the sink.

In the present work, we use Asqtad fermions for the sea quarks from configurations generated by the MILC collaboration. We then use domain wall fermions with an exact lattice chiral symmetry for the valence quarks. The resulting lattice theory should become a valid description of the full theory in the continuum limit provided this limit exists. These simulations extend the calculations we have already reported on in [10]. The current status of our lattice simulations is summarized in table 2. All working points are at a constant lattice spacing corresponding to $a^{-1} = 1.588$ GeV.

## 4. Moments of parton distributions

The lattice calculations of low moments of the nucleon parton distributions play multiple roles in the effort to understand the non-perturbative structure of hadrons in QCD. First, the lowest moments of the nucleon's parton distributions are interesting observables reflecting that the quark spin

| Volume $\Omega$ | Configs. | $(\mathbf{am_q})^{\text{Asqtad}}$ | $\mathbf{m}_{\text{PS}}$ / MeV |
|---|---|---|---|
| $20^3 \times 32$ | 425 | 0.050 | 790(2) |
| | 350 | 0.040 | 693(3) |
| | 564 | 0.030 | 594(2) |
| | 486 | 0.020 | 492(2) |
| | 655 | 0.010 | 354(2) |
| $28^3 \times 32$ | 271 | 0.010 | 352(1) |

**Table 2:** Summary of our working points and statistics for our hybrid calculations.

provides only a small fraction of the nucleon's spin and that only a small portion of the nucleon's momentum is carried by the quarks. Quark orbital motion and gluon contributions must account for the missing nucleon spin, and additionally the gluons must provide the remaining momentum within the nucleon. Therefore reliable non-perturbative QCD calculations of the moments of parton distributions are essential to the theoretical effort to understand nucleon structure.

Additionally the lattice calculation of moments of nucleon parton distributions will provide a benchmark test for the calculation of other hadronic observables because the calculations of moments can be compared directly with the corresponding experimental measurements of the nucleon. As lattice calculations are performed at light enough quark masses that controlled quantitative comparison with experimental results is achieved, then we will have confidence in the calculation of other hadronic matrix elements which may be poorly determined by experiment. As an example, the moments of generalized parton distributions or the large $Q^2$ limit of nucleon form factors discussed in Sections 5 and 6 will require varying levels of difficulty to measurement experimentally and the successful calculation of moments of ordinary parton distributions will allow for genuine predictions from lattice calculations for these and other observables.

**Lattice details**   The moments of parton distributions are determined by calculating matrix elements of the twist two operators in lattice QCD. For example the moments of the unpolarized and longitudinally polarized distributions are given by

$$\langle x^{n-1} \rangle_q p^{\{\mu_1} \cdots p^{\mu_n\}} = \frac{1}{2} \langle p, S | \overline{q} iD^{\{\mu_1} \cdots iD^{\mu_{n-1}} \gamma^{\mu_n\}} q | p, S \rangle \,,$$

$$\langle x^{n-1} \rangle_{\Delta q} S^{\{\mu_1} \cdots p^{\mu_n\}} = \frac{2}{n+1} \langle p, S | \overline{q} iD^{\{\mu_1} \cdots iD^{\mu_{n-1}} \gamma^{\mu_n\}} \gamma^5 q | p, S \rangle \,,$$

where the moments are defined as

$$\langle x^{n-1} \rangle_q = \int_{-1}^{1} dx \, x^n q(x) = \int_0^1 dx \, x^n (q(x) - \overline{q}(x)) \,,$$

$$\langle x^{n-1} \rangle_{\Delta q} = \int_{-1}^{1} dx \, x^n \Delta q(x) = \int_0^1 dx \, x^n (\Delta q(x) + \Delta \overline{q}(x)) \,.$$

These moments are encoded in the generalized form factors discussed in Section 2 as

$$A_{n0}^q(0) = \langle x^{n-1} \rangle_q$$
$$\tilde{A}_{n0}^q(0) = \langle x^{n-1} \rangle_{\Delta q} \,.$$
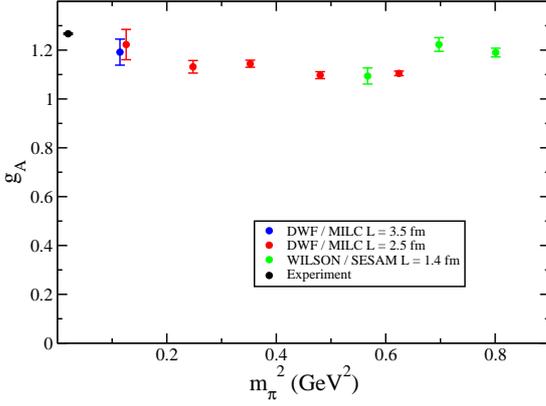
**Figure 1:** $\langle 1 \rangle_{\Delta u - \Delta d}$
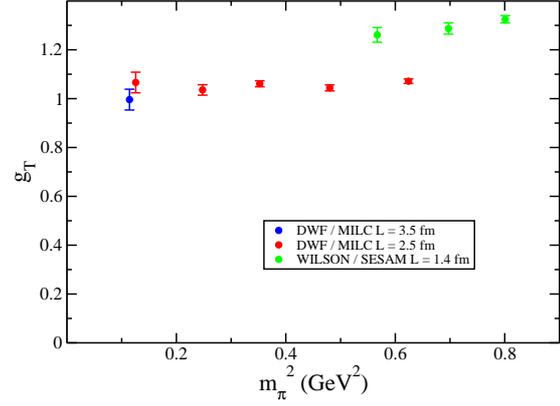


**Figure 2:** $\langle 1 \rangle_{\delta u - \delta d}$

Additionally the moments of the transversity distribution, labeled by $\delta q$ in the following, can be calculated with similar expressions. All the remaining details can be found in [12].

All but the most trivial moments must be renormalized at some scale. With the exception of the axial coupling, all the moments discussed here are matched in the chiral limit to $\overline{MS}$ at $\mu = 2$ GeV using one-loop perturbation theory [13]. The one exception, the axial coupling, is renormalized non-perturbatively in the chiral limit using the five dimensional domain wall conserved axial current.

Figures 1 through 4 show the results from this calculation and from a previous calculation with Wilson quarks [12]. With one exception the points reading from left to right denote the following: point 1 is the experimental value, point 2 is the 3.5 fm domain wall calculation, points 3-6 and 8 are the 2.5 fm domain wall calculations, and points 7 and 9-10 are the 1.5 fm Wilson calculations. The one exception is that Figure 2 lacks the experimental value but is otherwise identical.

**Axial and tensor couplings** As our calculations enter the chiral regime, the axial coupling is a particularly good benchmark observable. Physically $g_A = \langle 1 \rangle_{\Delta u - \Delta d}$ represents the non-singlet contribution of light quark spins to the nucleon spin. Furthermore it is well determined in neutron $\beta$ decay, and more importantly it has no disconnected diagrams and thus is unambiguously calculable with current lattice calculations. Figure 1 illustrates our recent calculations of $g_A$ along with our group's previous calculations at heavier quark masses [12]. As mentioned earlier, the renormalization constant is calculated non-perturbatively in the chiral limit and is determine to be $Z_A = 1.0751(11)$. As Figure 1 illustrates very clearly, we are making significant progress in calculating $g_A$ at the physical quark masses. A tentative calculation by our group to study the chiral extrapolation of $g_A$ as a function of the pion mass is given in [14] and will be examined carefully in an upcoming publication. Additionally, the axial coupling provides a good test of finite size effects because previous calculations [15] have shown that $g_A$ is particularly sensitive to the finite size of a calculation. Figure 1 shows our results for volumes of $(2.5 \text{ fm})^3$ and $(3.5 \text{ fm})^3$ at the lightest quark mass indicating that finite size effects appear to be smaller than the statistical accuracy of our calculations.

Our corresponding results for the non-singlet tensor charge, $g_T = \langle 1 \rangle_{\delta u - \delta d}$, are shown in Fig-
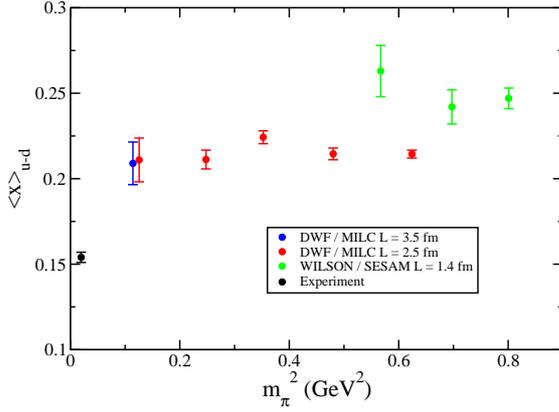
**Figure 3:** $\langle x \rangle_{u-d}$
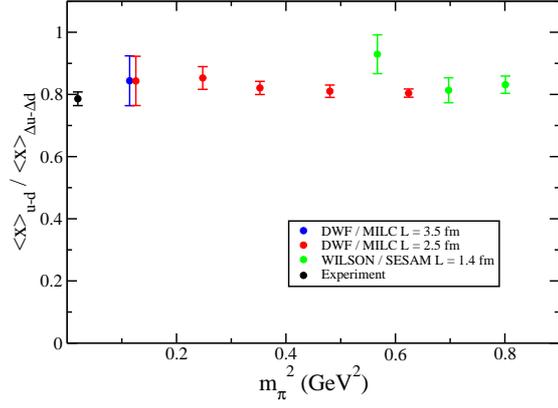


**Figure 4:** $\langle x \rangle_{u-d} / \langle x \rangle_{\Delta u - \Delta d}$

ure 2 at each of the same pion masses as in Figure 1. The most noteworthy observation is that the discrepancy between the Wilson and domain wall results is greater than for the axial charge. Finite size effects and lattice artifacts may account for the discrepancy, but as suggested in [16] renormalization may also be a significant effect. A similar mismatch is observed for the momentum fraction as well, and we plan to study the non-perturbative renormalization of these operators to investigate the discrepancy.

**Unpolarized and polarized momentum fractions**   Unlike the axial coupling, the momentum fraction remains a challenge for contemporary lattice calculations. Simply put, nearly all lattice calculations to date overestimate the momentum fraction, which represents the quark contribution to the nucleon's momentum. Hence lattice calculations do not yet seem to correctly account for the sizable fraction of momentum carried by gluons in the chiral limit. Thus it appears that the main obstacle in correctly determining the physical value of $\langle x \rangle$ is to calculate at sufficiently light quark masses such that chiral perturbation theory can be used to reliably extrapolate to the physical masses [17]. Figure 3 illustrates our groups progress toward this goal. In this figure we focus on the non-singlet contribution, $\langle x \rangle_{u-d}$, to avoid complications arising from disconnected diagrams. The issues involved in correctly matching the previous heavier Wilson quark calculations to the current domain wall calculations were discussed earlier with regard to the tensor charge, and the same comments apply here. It is worthwhile to note that, even though the lattice calculations at lighter pion masses do not yet show any significant curvature, the lighter results do show a systematic shift toward the experimental result.

Despite the challenges involved in $\langle x \rangle$, it was noted in [18] that the ratio of unpolarized to longitudinally polarized momentum fractions yields an observable which appears to be less sensitive to the issues which still plague $\langle x \rangle$ alone. In particular with a chiral action the renormalization of operators which differ solely by an insertion of $\gamma_5$ is identical. Hence the ratio $\langle x \rangle_{u-d} / \langle x \rangle_{\Delta u - \Delta d}$ requires no renormalization. Furthermore as illustrated in Figure 4 the finite size and pion mass dependence appears to strongly cancel in this ratio as well.
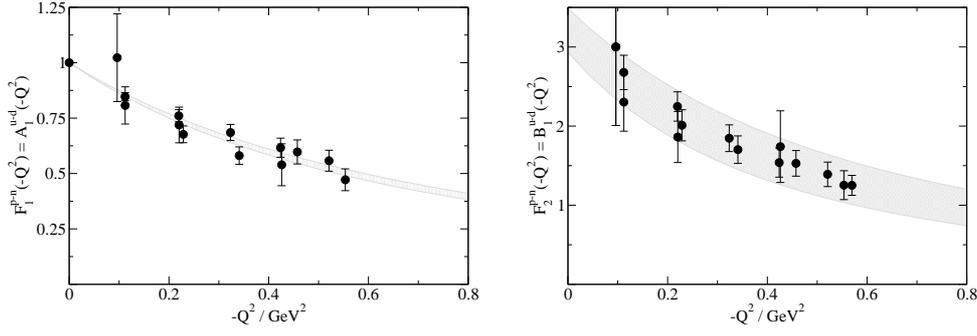
**Figure 5:** The electromagnetic form factors of the nucleon at small values of $Q^2$.

## 5. Moments of generalized parton distributions

In the following, we only present numerical results from the lightest working point on the $28^3 \times 32$ lattice. Hence, these simulations correspond to a pion mass of $m_\pi = 352$ MeV. Furthermore, the results presented in this section have not yet been renormalized in the $\overline{\text{MS}}$-scheme, but in the lattice regularization of our action at the scale given in section 3. They are intended as a test of our lattice technology and not to be compared directly to experimental data so far.

Our results for the electromagnetic form factors of the nucleon, $F_1^{\text{p-n}}(t) = A_{10}^{\text{u-d}}(t)$ and $F_2^{\text{p-n}}(t) = B_{10}^{\text{u-d}}(t)$, are shown in figure 5.

The three generalized form factors appearing in the parameterization of the nucleon energy-momentum tensor, cf. eq. (2.2), are shown in figure 6.

An important qualitative finding of [7] was that the transverse structure of the nucleon is indeed not described properly by the assumption that the $t$-dependence factorizes from the $x$ and $\xi$ dependence of a GPD. This ansatz has been made in several phenomenological studies and turned out to be inaccurate. We reproduced a key result in figure 7 and find, again, that the transverse shape of the nucleon becomes narrower as the longitudinal momentum fraction, $x$, increases.

## 6. Form factors at large momentum transfer

**Motivation** The isovector part of the electromagnetic form factors of the nucleon for momentum transfers less than 1 GeV have already been discussed in section 5 and shown in figure 5. The shaded bands are a dipole fit to the lattice data and consistent with the phenomenological notion that the form factors generally follow the dipole form

$$G_D(Q^2) \propto \left(1 - \frac{Q^2}{\Lambda^2}\right)^{-2}, \qquad \Lambda^2 \approx 0.71 \text{ GeV}^2 \qquad (6.1)$$

in this range of momentum transfers. This can be seen directly from the simple parameterization of the existing experimental data for Sachs form factors by J. J. Kelly [19]. In our normalization, the Sachs form factors are determined by the Dirac and Pauli form factors as

$$G_E(Q^2) = F_1(Q^2) - \tau F_2(Q^2), \quad G_M(Q^2) = F_1(Q^2) + F_2(Q^2), \quad \tau = \frac{-Q^2}{4m_N^2}. \qquad (6.2)$$
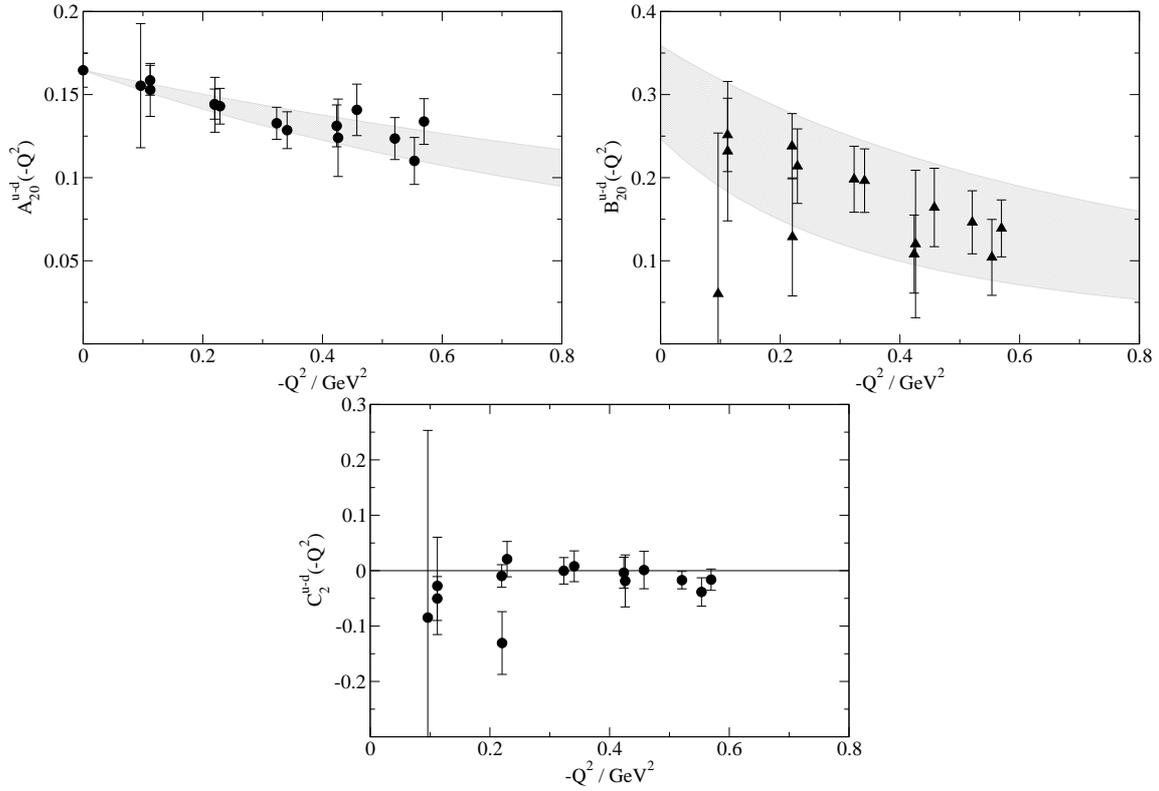
**Figure 6:** The three GFFs, $A_{20}$, $B_{20}$, and $C_2$, appearing in the parameterization of the nucleon energy-momentum tensor. The data is unrenormalized and would be corrected by about 20% if renormalized in the $\overline{\text{MS}}$ scheme at a scale of $\mu_R = 2$ GeV.
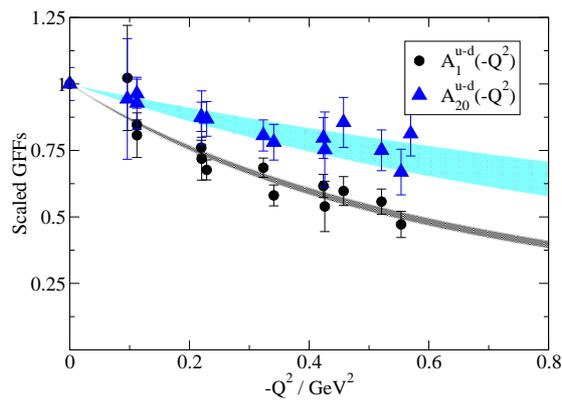


**Figure 7:** The comparison of the scaled GFFs $A_{10}(t)$ and $A_{20}(t)$ signaling the non-factorization of the longitudinal and transverse momentum dependence.
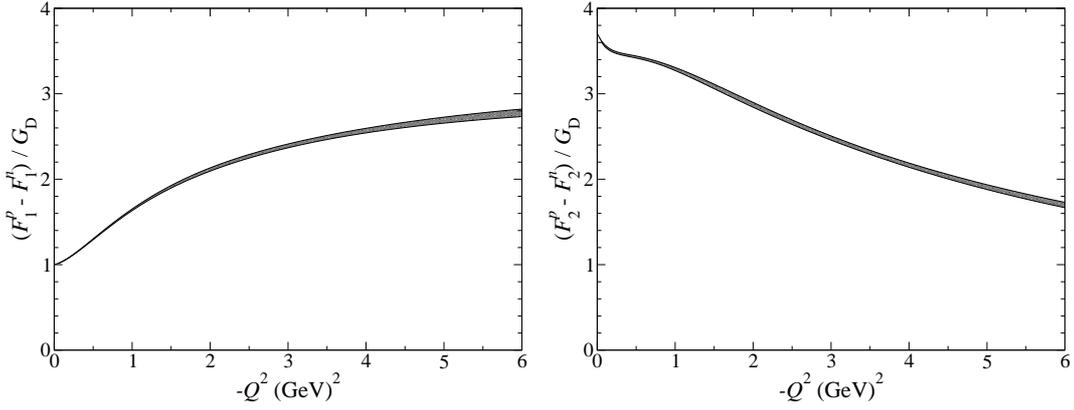
**Figure 8:** Experimental parameterizations of isovector $F_1$ (Dirac) and $F_2$ (Pauli) form factors. Dipole form factor $G_D$ has $\Lambda^2$=0.71 GeV$^2$ [19].
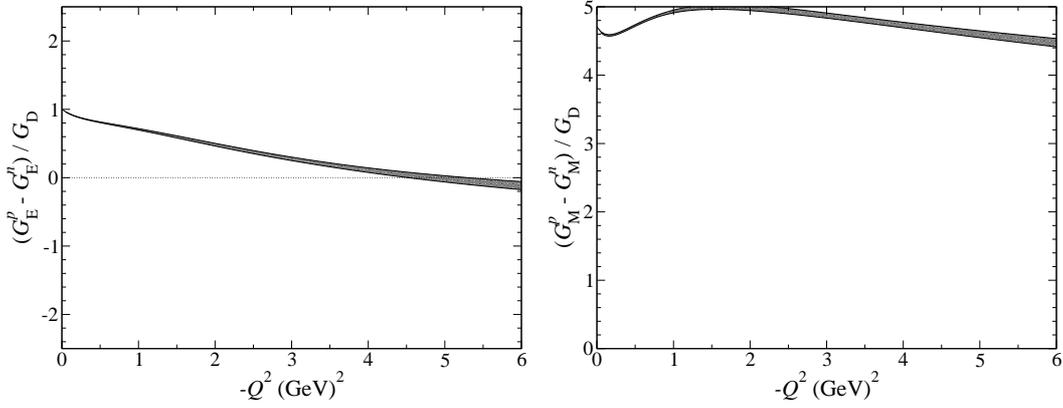


**Figure 9:** Experimental parameterizations of isovector Sachs $G_E$ (electric) and $G_M$ (magnetic) form factors. Dipole form factor $G_D$ has $\Lambda^2$=0.71 GeV$^2$ [19].

We can invert equation (6.2), form isovector combinations and, using the parameterization [19] and its covariance matrix [20], produce curves derived from experimental data for direct comparison with lattice isovector form factors. Figure 8 shows the 1 $\sigma$ bands for the Dirac and Pauli form factors. Figure 9 shows similar 1 $\sigma$ bands for the Sachs electric and magnetic form factors.

While all experimental curves show some variation with $Q^2$ relative to the dipole form, the most intriguing feature is the apparent zero-crossing of $G_E^p - G_E^n$ around $-Q^2 \approx 5$ GeV$^2$. This is similar to the possible zero-crossing of $G_E^p/G_M^p$ around $-Q^2 \approx 10$ GeV$^2$ as suggested by various extrapolations of the data from recent polarization transfer experiments [21, 22, 23, 24, 25]. It appears that by focusing on the isovector parts of form factors it may be possible for lattice calculations to predict the vanishing of the electric form factor at lower $Q^2$ than previously thought possible. Thus, the purpose of this section is to estimate what level of statistics are required to achieve a significant measurement of a negative electric form factor at $-Q^2 \approx 6$ GeV$^2$.

Another motivation for calculating form factors in the regime $-Q^2 \gg 1$ GeV$^2$ is to test the predictions of perturbative QCD (pQCD) at asymptotically high $Q^2$ [26, 27]. In pQCD, the nucleon

MILC_2064f21b681m030m050, *a*=0.124 fm, $m_{\mathrm{PS}}$=594 MeV
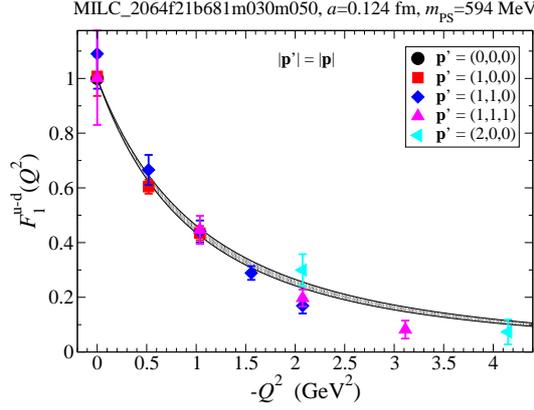


**Figure 10:** Isovector Dirac form factor in the Breit frame ($|\vec{p}'| = |\vec{p}|$) for several sink momenta $\vec{p}'$ *vs.* a dipole fit of the data.

form factors are expected to scale: $F_1 \sim Q^{-4}$, $F_2 \sim Q^{-6}$ as $Q^2 \to \infty$. So, it is easy to form scaling ratios which should be roughly constant at higher momentum transfers. Ratios like $Q^2 F_2/F_1$ and $G_E/G_M$ should scale but have not yet been observed to do so. Recently, it has been noted [28, 29] that the ratio $F_2/F_1$ has an additional logarithmic factor: $Q^2 F_2/F_1 \sim \log^2(Q^2/\Lambda^2)$ where $\Lambda \approx$ 300 MeV seems to roughly restore scaling of experimental data in the range $-Q^2 = 2 - 6 \text{ GeV}^2$.

A word of caution is in order with regards to apparent scaling of the experimental data having its origins in pQCD scaling in the asymptotic regime. In a recent lattice calculation of the pion electromagnetic form factor $F_\pi(Q^2)$ [30] in the same hybrid scheme as described in section 3, scaling was observed for $F_\pi(Q^2)$ as predicted by pQCD. In the case of the pion, it is also possible to compute the asymptotic normalization and the data did not yet agree with the pQCD prediction. Thus, scaling alone is not sufficient to establish the reliability of pQCD calculations of nucleon form factors.

**Exploring higher $Q^2$ on the lattice**   To estimate the computational costs of computing nucleon electromagnetic form factors to $-Q^2 \sim 6 \text{ GeV}^2$, we computed sequential propagators on 282 configurations separated by 12 MILC HMD trajectories, at $m_{\mathrm{PS}} = 594(2)$ MeV, half of those listed in table 2, for higher sink momenta $\vec{p}' = (1,1,0)$, $(1,1,1)$ and $(2,0,0)$. For this study, we focused on computing in the Breit frame ($\vec{p}' = -\vec{p}$) as past experience has shown that computed form factors have smaller statistical variance than other momentum combinations at the same $Q^2$. Our results for $F_1^{u-d}(Q^2)$ are shown in figure 10 and are consistent with dipole scaling over the entire range of $Q^2$.

In figure 11, we plot the relative error of $F_1^{u-d}(Q^2)$ in the Breit frame. We fit the points to several functional forms with three or less free parameters in order to extrapolate our results to higher sink momenta. The polynomial curve shown was the best representation of the data we found. This form is motivated by the following picture. $F_1$ decreases as $Q^{-4} \propto n^{-4}$ in the Breit frame. If the statistical noise in our matrix element construction is independent of the magnitude of the sink momenta, then the relative error should increase as $n^4$ which is consistent with our calculation.
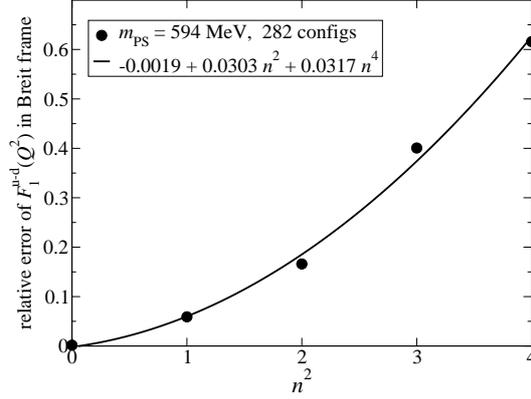
**Figure 11:** Relative error of the isovector Dirac form factor *vs.* sink momenta $\vec{p}' = 2\pi\vec{n}/L$, where $n^2 = \vec{n}\cdot\vec{n}$, at fixed $m_{\text{PS}} = 594(2)$ MeV.

Because we would like to establish whether a zero-crossing occurs around $-Q^2 = 5$ GeV$^2$ for the isovector electric form factor, we would like to set a goal of achieving 30% relative errors up to 6 GeV$^2$. For $\vec{p}' = (2,0,0)$, $n^2 = 4$ and $-Q^2 = 4.15$ GeV$^2$ the relative error is 62%. Reducing the relative error to 30% at this $Q^2$ should therefore require four times the number of configurations, two times more than our current dataset.

To reach 6 GeV$^2$ requires a sink momenta of $\vec{p}' = (2,2,0)$, $n^2 = 8$ and our extrapolation predicts we should find a relative error of 227% on our set of 282 configurations. To reduce this relative error to 30% should require 57 times as many configurations, on the order of 200,000 MILC HMD trajectories! Since it is unlikely that this ensemble will be extended by so many trajectories, achieving our goals will require some other technique to reduce the variance of matrix elements at higher $Q^2$.

Another important question is how does the relative error of the form factors depend on the dynamical pion mass at fixed $Q^2$. In figure 12 we show the relative error for $F_1^{u-d}(Q^2)$ as a function of the pion mass in the Breit frame at fixed sink momenta $\vec{p}' = (1,0,0)$. Note that the box size is held fixed in lattice units ($L=20$) and thus $m_{\text{PS}}L$ varies but always $m_{\text{PS}}L > 4$. As before, we attempted to fit various functional forms to the data and the form which best fit the data is plotted. In this case, we were unable to find any other functional form with three or fewer parameters which could fit the data with any comparable accuracy. We do not currently have a good physical motivation for this functional form except to note that the scale at which the divergence sets in is approximately 250 MeV, comparable with the scale at which other chiral extrapolations of hadronic matrix elements typically show substantial curvature. This figure clearly reiterates the need to identify some other technique for reducing the variance of hadronic matrix elements at higher $Q^2$.

## 7. Summary and outlook

We have demonstrated selected results for the structure of the nucleon at light quark masses using our hybrid approach. We have focused on a specific sample at one working point of our simulations to demonstrate the qualitative behavior of the generalized form factors. The results are in
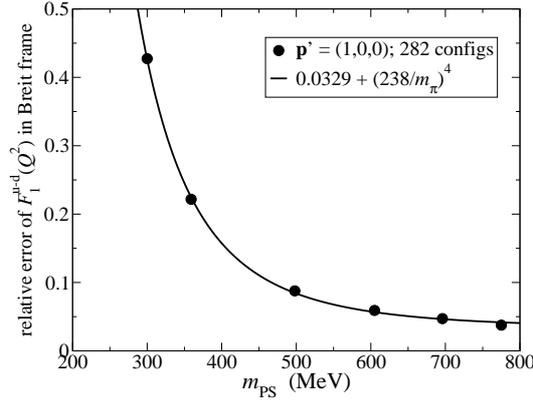
**Figure 12:** Relative error of the isovector Dirac form factor *vs.* pion mass at fixed sink momentum.

qualitative agreement with previous findings and we did not encounter major problems during our runs. We then focused on a direct comparison of several moments of the forward limit of parton distributions to experiment. These results included our entire data set and the direct comparison to experimental data has given quantitative agreement in several cases once appropriate chiral extrapolations have been considered. Finally, we have explored the possibility of exploring the regime of larger virtual momentum transfers in the case of the nucleon form factors.

The encouraging results make us confident that the hybrid approach is indeed promising to bridge the gap between current lattice data and the regime where chiral perturbation theory is applicable. These results are therefore of great importance to the qualitative and quantitative understanding of hadronic matrix elements.

Before the advent of light dynamical overlap and domain-wall calculations we will provide a complete analysis of selected quantities like the nucleon axial coupling [31], light hadron spectroscopy [32], and all accessible moments of generalized parton distributions [33].

## Acknowledgments

## References

[1] D. Müller, D. Robaschik, B. Geyer, F. M. Dittes and J. Horejsi, Fortsch. Phys. **42**, 101 (1994).

X. D. Ji, Phys. Rev. Lett. **78**, 610 (1997).
A. V. Radyushkin, Phys. Rev. D **56**, 5524 (1997).

[2] M. Diehl, Phys. Rept. **388**, 41 (2003).
A. V. Radyushkin, Phys. Rev. D **56**, 5524 (1997).

[3] N. Mathur, S. J. Dong, K. F. Liu, L. Mankiewicz and N. C. Mukhopadhyay, Phys. Rev. D **62**, 114504 (2000).

[4] M. Göckeler, R. Horsley, D. Pleiter, P. E. L. Rakow, A. Schäfer, G. Schierholz and W. Schroers [QCDSF Collaboration], Phys. Rev. Lett. **92**, 042002 (2004).

[5] P. Hägler, J. Negele, D. B. Renner, W. Schroers, T. Lippert and K. Schilling [LHPC Collaboration], Phys. Rev. D **68**, 034505 (2003).

[6] M. Diehl, T. Feldmann, R. Jakob and P. Kroll, Eur. Phys. J. C **39**, 1 (2005).

[7] P. Hägler, J. W. Negele, D. B. Renner, W. Schroers, T. Lippert and K. Schilling [LHPC Collaboration], Phys. Rev. Lett. **93**, 112001 (2004).
M. Göckeler *et al.* [QCDSF Collaboration], Nucl. Phys. Proc. Suppl. **128**, 203 (2004).
M. Göckeler *et al.* [QCDSF Collaboration], Nucl. Phys. Proc. Suppl. **135**, 156 (2004).
J. W. Negele *et al.* [LHPC Collaboration], Nucl. Phys. Proc. Suppl. **129**, 910 (2004).
B. Bistrovic *et al.* [LHPC Collaboration], arXiv:hep-lat/0509101.

[8] W. Schroers *et al.* [LHPC collaboration], Nucl. Phys. Proc. Suppl. **129**, 907 (2004).
P. Hägler, J. W. Negele, D. B. Renner, W. Schroers, T. Lippert and K. Schilling [LHPC Collaboration], Eur. Phys. J. A **24S1**, 29 (2005).

[9] M. Göckeler *et al.* [QCDSF Collaboration], arXiv:hep-lat/0501029.
M. Göckeler *et al.* [QCDSF Collaboration], arXiv:hep-lat/0507001.
A. Schäfer *et al.* [QCDSF Collaboration], these proceedings.

[10] D. B. Renner *et al.* [LHP Collaboration], Nucl. Phys. Proc. Suppl. **140**, 255 (2005).

[11] D. Brömmel *et al.*, arXiv:hep-lat/0509133. These proceedings.

[12] D. Dolgov *et al.* [LHPC Collaboration], Phys. Rev. D **66**, 034506 (2002).

[13] B. Bistrovic *et al.*, (2005), in preparation.

[14] D. B. Renner, arXiv:hep-lat/0508008.
D. B. Renner, J. Phys. Conf. Ser. **9**, 264 (2005).
W. Schroers, Nucl. Phys. A **755**, 333 (2005).

[15] S. Sasaki *et al.* [RBCK Collaboration], Phys. Rev. D **68**, 054509 (2003).

[16] T. Streuer *et al.* [QCDSF Collaboration], these proceedings.

[17] W. Detmold, W. Melnitchouk, J. W. Negele, D. B. Renner and A. W. Thomas, Phys. Rev. Lett. **87**, 172001 (2001).

[18] K. Orginos, T. Blum and S. Ohta, arXiv:hep-lat/0505024.

[19] J. J. Kelly, Phys. Rev. C **70**, 068202 (2004).

[20] J. J. Kelly, private communication.

[21] B. D. Milbrath *et al.* [Bates FPP collaboration], Phys. Rev. Lett. **80**, 452 (1998) [Erratum-ibid. **82**, 2221 (1999)].

[22] T. Pospischil *et al.* [A1 Collaboration], Eur. Phys. J. A **12**, 125 (2001).

[23] O. Gayou *et al.* [Jefferson Lab Hall A Collaboration], Phys. Rev. Lett. **88**, 092301 (2002).

[24] O. Gayou *et al.*, Phys. Rev. C **64**, 038202 (2001).

[25] V. Punjabi *et al.*, Phys. Rev. C **71**, 055202 (2005) [Erratum-ibid. C **71**, 069902 (2005)].

[26] S. J. Brodsky and G. R. Farrar, Phys. Rev. D **11**, 1309 (1975).

[27] G. P. Lepage and S. J. Brodsky, Phys. Rev. D **22**, 2157 (1980).

[28] S. J. Brodsky, arXiv:hep-ph/0208158.

[29] A. V. Belitsky, X. d. Ji and F. Yuan, Phys. Rev. Lett. **91**, 092003 (2003).

[30] F. D. R. Bonnet, R. G. Edwards, G. T. Fleming, R. Lewis and D. G. Richards [Lattice Hadron Physics Collaboration], Phys. Rev. D **72**, 054506 (2005).

[31] [LHPC Collaboration], in preparation.

[32] [LHPC Collaboration], in preparation.

[33] [LHPC Collaboration], in preparation.